INCREMENTAL DYNAMIC ANALYSIS WITH TWO COMPONENTS OF MOTION FOR A 3D STEEL STRUCTURE

D. Vamvatsikos[1]

ABSTRACT

Incremental dynamic analysis (IDA) is employed to evaluate the seismic performance of a 20-story steel space frame under biaxial seismic loading. Originally developed for planar frames and uniaxial loading, the IDA framework is now extended to 3D. This involves performing a series of nonlinear timehistory analyses under a suite of ground motion records by equally scaling both components of each record to several levels of intensity and recording the structural response. The structure is thus forced to show its complete spectrum of behavior from elasticity to final global instability for combinations of intensities in the two directions. Using proper intensity measures (e.g., spectral acceleration coordinates of the record components) and engineering demand parameters (e.g., maximum interstory drifts), the familiar IDA curves plus novel IDA surfaces are created, representing the structural response and its statistical summary at any intensity level. These enable a rational definition of limit-states and the calculation of the resulting capacities in a manner consistent with current IDA techniques. A powerful analysis procedure is thus created that is capable of thoroughly assessing the seismic performance of 3D structures and may serve as a solid benchmark for evaluating the accuracy of simpler methods.

Introduction

It is common practice in earthquake engineering to economize by ignoring the spatial nature of structures. Using two-dimensional (2D) models and associated analysis methods has become the standard, allowing significant reductions in the analysis complexity by effectively ignoring the three-dimensional (3D) structural interaction and the biaxial nature of seismic loading. Nevertheless, the rapid evolution of computing power available to the practicing user is finally starting to close the gap, making complex 3D dynamic analyses feasible. What is lacking is a methodology to organize such analyses and make sense out of the abundant results.

Incremental dynamic analysis (IDA) (Vamvatsikos and Cornell 2002) is an analysis method that has recently emerged as a promising tool for thoroughly evaluating the seismic performance of structures. Originally developed for 2D structures, it involves subjecting a

[1]Lecturer, Dept. of Civil & Environmental Engineering, Univ. of Cyprus, 1678 Nicosia, Cyprus

structural model to a suite of ground motion records, each scaled to several intensities (as measured by the intensity measure, IM), and recording the responses (measured by engineering demand parameters, EDPs) at each level to form IDA curves of response versus intensity. Allowing for the transparent definition of limit-states and the accurate estimation of the probabilistic distribution of the associated capacities, it forms a reliable but computer-intensive platform for performance-based earthquake engineering. While the original framework set forth by Vamvatsikos and Cornell (2002) does encompass 3D applications, most studies so far have been restricted to 2D structures, precisely due to the enormous computing load. Actually, applying IDA in 3D is only an exercise in post-processing the results of the 3D dynamic analyses. However it becomes quite complicated and extremely interesting when we contemplate the issue of using a vector of intensity measures, one for each horizontal component of the ground motion. Using a 20-story steel space frame as an example, we will present one by one the steps needed to perform a complete seismic evaluation in three dimensions.

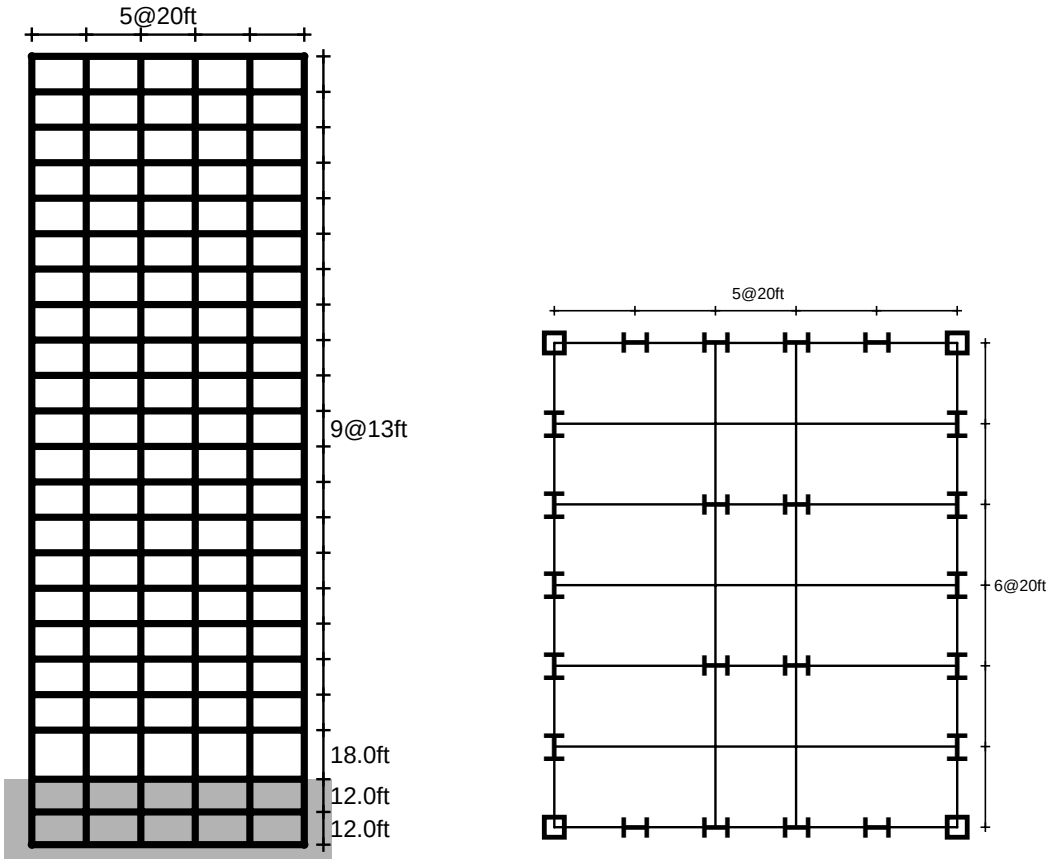

Figure 1. Profile and plan of the 20-story frame.

Structure and Model Description

The structure considered is a steel moment resisting frame, five-by-six bays in plan, 20-stories high, with a two-storey basement (Fig. 1). The frame has been designed for a Los Angeles site, following the 1997 NEHRP (National Earthquake Hazard Reduction Program) provisions (Gupta and Krawinkler 1999, Foutch and Yun 2002). A centerline model with lumped-plasticity

beam-column elements was formed using the OpenSEES platform (McKenna et al 2001). All columns remain elastic, but ductile plastic hinges are allowed to form at the beam ends. Geometric nonlinearities in the form of P-Δ effects were considered while the internal gravity frames have been explicitly incorporated. The fundamental periods of the resulting model are $T_{1x} = 3.6\,\text{sec}$ in the short x-direction (five bays) and $T_{2x} = 3.3\,\text{sec}$ in the long y-direction (six bays); it is obviously a higher-mode sensitive structure, with only a mild asymmetry in the two principal directions.

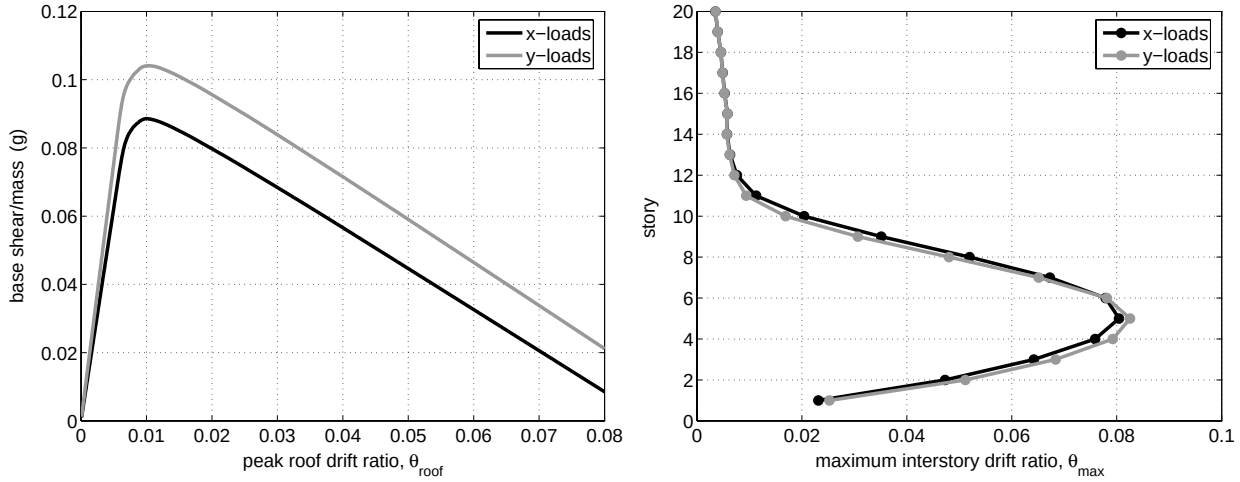

(a) (b)

Figure 2. (a) The pushover curves and (b) the interstory drift profiles for $\theta_{\text{roof}} = 3\%$ and a parabolic load pattern pushing along the x (short) or the y (long) direction. The responses are recorded along the direction of the loading.

As means of understanding the expected behavior of the structure under dynamic loading, we perform static pushover analysis (SPO) along each of the principal directions. The resulting SPO curves appear in Fig. 2a. There it becomes evident that P-Δ effects are dominating almost immediately after yielding and bring this tall structure to collapse around 9-10% roof drift θ_{roof}. This is indeed an unrealistic number, but it should be expected for such a ductile frame. Similar high values are attained by the peak interstory drift, as seen in the profile shown in Fig. 2b for $\theta_{\text{roof}} = 3\%$. There is an obvious concentration of deformations that occurs in the lower stories, forming a characteristic "belly" when pushing in any of the two directions. Keeping in mind the connection between the SPO and the IDA, established by Vamvatsikos and Cornell (2002), we should expect that the negative stiffness appearing in the SPO curves will manifest itself as numerical instability, i.e., global collapse, in the IDA curves.

Performing IDA for 3D Structures

Performing IDA on a structural model requires a suite of ground motion records to represent the seismic threat, an efficient intensity measure (IM) to scale the records and an appropriate choice of engineering demand parameters (EDPs) to adequately characterize the structural response. All three elements are necessary ingredients of IDA and perhaps the most important difference in selecting them when doing 3D versus 2D analysis is that we now need two components of ground motion instead of just one.

Therefore, we are going to use twenty-six ground motion records with two horizontal components each, shown in Table 1. These were selected from a relatively narrow magnitude and distance bin, having moment magnitude within 6.5 – 6.9 and closest distance to fault rupture ranging from 13.9 to 37.7km. They have all been recorded on firm soil and bear no marks of near-fault directivity, generally placing them in the "regular" ground motion category.

Table 1. The suite of twenty ground motion records (two components each) used. First component (1) is applied along the x-axis and the second (2) along the y-axis of the model.

Event Station	R [a] (km)	Soil [b]	Φ_1 [c] (deg)	φ_2 [d] (deg)	PGA_1 (g)	PGA_2 (g)
Superstition Hills 1987 (M=6.7) [d]						
1. El Centro Imp. Co Cent	13.9	C,D	000	090	0.36	0.26
San Fernando, 1971 (M=6.6)						
2. LA Hollywood Sto Lot	21.2	C,D	090	180	0.21	0.17
Imperial Valley 1979 (M=6.5)						
3. Chihuahua	28.7	C,D	012	282	0.27	0.25
4. Plaster City	31.7	C,D	045	135	0.04	0.06
5. Compuertas	32.6	C,D	015	285	0.19	0.15
6. El centro Array #12	18.2	C,D	140	230	0.14	0.12
7. El centro Array #13	21.9	C,D	140	230	0.12	0.14
8. Westmoreland Fire Station	15.1	C,D	090	180	0.07	0.11
9. El centro Array #1	15.5	C,D	140	230	0.14	0.13
Northridge 1994 (M=6.7)						
10. Leona Valley #2	37.7	C,–	000	090	0.09	0.06
11. Lake Hughes #1	36.3	C,C	000	090	0.09	0.08
12. LA Hollywood Sto FF	25.5	C,D	090	360	0.23	0.36
13. LA Baldwin Hills	31.3	B,B	090	360	0.24	0.17
14. Canoga Park - Topanga Can	15.8	C,D	106	196	0.36	0.42
15. LA N Faring Rd	23.9	C,B	000	090	0.27	0.24
16. LA Fletcher Dr	29.5	C,D	144	234	0.16	0.24
17. LA Centinela St	30.9	C,D	155	245	0.47	0.32
18. Glendale Las Palmas	25.4	C,C	177	267	0.36	0.21
Loma Prieta 1989 (M=6.9)						
19. Hollister Diff Array	25.8	–,D	165	255	0.27	0.28
20. WAHO	16.9	–,D	000	090	0.37	0.64
21. Halls Valley	31.6	C,C	000	090	0.13	0.10
22. Agnews State Hospital	28.2	C,D	000	090	0.17	0.16
23. Anderson Dam Downstrm	21.4	B,D	270	360	0.24	0.24
24. Coyote Lake Dam Downstrm	22.3	B,D	195	285	0.16	0.18
25. Sunnyvale Colton Ave	28.8	C,D	270	360	0.21	0.21
26. Hollister South & Pine	28.8	–,D	000	090	0.37	0.18

[a] Closest distance to fault rupture
[b] USGS, Geomatrix soil class
[c] Component orientation
[d] Moment magnitude

When performing the analyses it is important to select an initial IM for the scaling of the records that achieves good correlation with collapse and a relatively low dispersion in the collapse IM-values (the flatlines); thus the IDA curves can be traced efficiently (Vamvatsikos and Cornell 2005). A mediocre choice is not a problem when using high-performance IDA-tracing algorithms like *hunt & fill* (Vamvatsikos and Cornell 2004), but a very poor IM-choice may increase the number of runs required to get a reasonable resolution. If we were to choose a single scalar IM for the 20-story building it would make perfect sense to select the dominant period in any direction. Therefore we choose as the 5%-damped first-mode spectral acceleration of the *x*-axis component, $S_{ax}(T_{1x},5\%)$. This choice will not restrict us in any sense when post-processing the results, it is only used for the scaling of the records when performing IDA and may later be replaced by any other scalable IM without needing to rerun the dynamic analyses.

Selecting the EDP is relatively straightforward for this space frame. Since maximum interstory drifts are generally considered to correlate well with story damage, we choose to monitor the maximum peak SRSS drift $\theta_{s\max}$, i.e., the maximum over all stories of the peak of the square-root-sum-of-squares (or vector sum) of each story's instantaneous drifts in the two principal directions. This has already seen use in the literature to capture the 3D response of space frames (e.g., Wen and Song 2002) and we expect it will provide a reasonable EDP, comparable to the maximum interstory drift used for 2D buildings. Having selected the EDP, the IM and the records, all that remains to do is run the nonlinear dynamic analyses and each time recover the single $\theta_{s\max}$ value for post-processing.

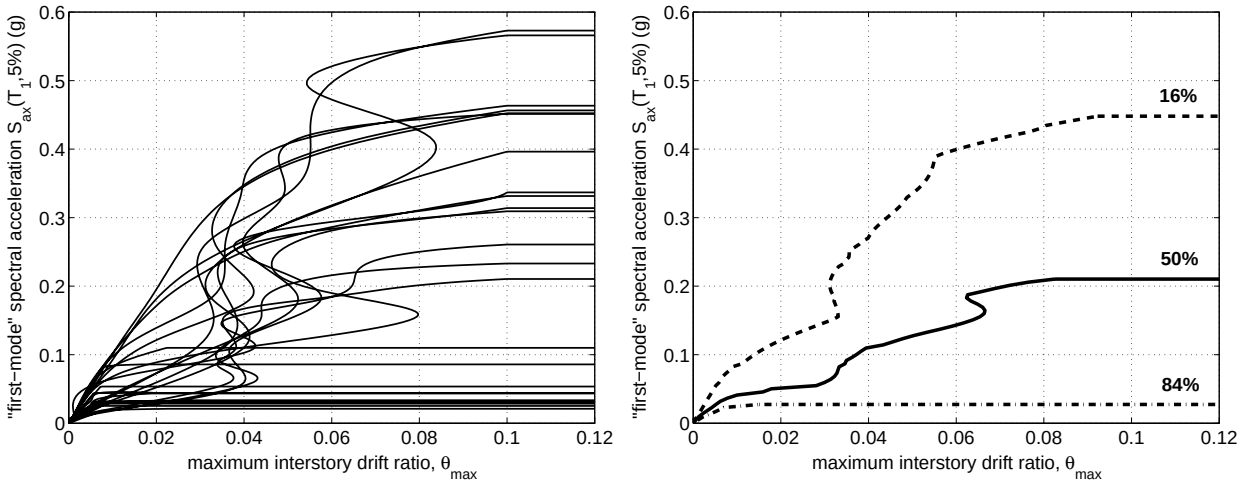

Figure 3. The twenty-six IDA curves for the maximum interstory drift ratio (a) and the summarization into 16, 50 and 84% fractiles (b).

Postprocessing with a Scalar Intensity Measure

Each analysis produces a pair of intensity versus response. These are discrete points in the IM-EDP plane which can be interpolated with a flexible spline scheme (Vamvatsikos and Cornell 2004) to produce twenty-six IDA curves, one for each record, as shown in Fig. 3a.

Perhaps the most striking characteristic to observe is the flatlines, occurring at widely dispersed intensities, ranging from $S_{ax}(T_{1x},5\%)$=0.03g up to 0.6g. These flatlines set the maximum IM limit that the frame can withstand, before global instability takes place.

Summarizing the IDA curves to produce the distribution of $\theta_{s\max}$ demands given $S_{ax}(T_{1x},5\%)$ is performed in the same way as in 2D frames. By calculating cross-sectional fractiles of the EDP at each level of intensity we can estimate the 16, 50 and 84% fractile IDA curves, appearing in Fig. 3b. In all cases though there is a considerable dispersion, in excess of 100%, even with this reasonable choice for an IM. Still, this should be expected as we have neglected the intensity of the *y*-axis component of the ground motion, which may well account for some of the observed record-to-record variability. To rectify this requires the introduction of a secondary IM, thus forming a vector of two, a non-trivial issue that deserves to be discussed in its own section.

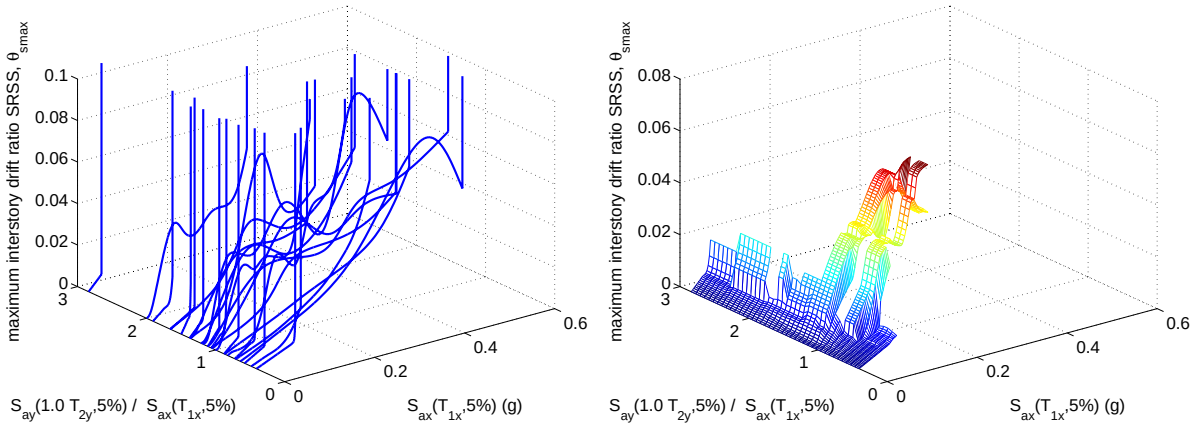

Figure 4. The twenty-six IDA curves for the maximum interstory drift ratio for a vector IM (a) and their summarization into a median surface (b).

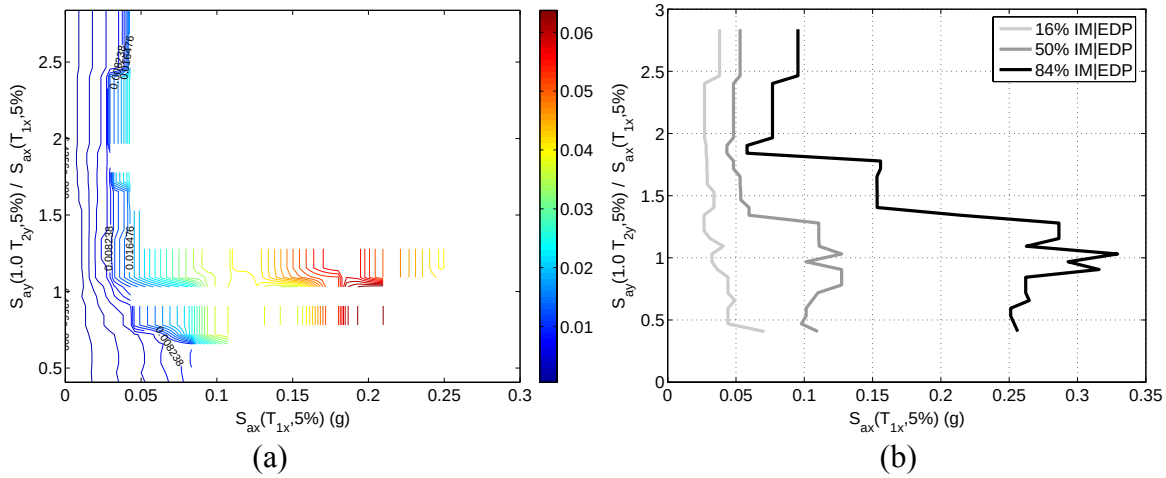

Figure 5. (a) Contours of the median surface from Fig. 4b and (b) 16, 50 and 84% capacity lines (or contours) for $\theta_{s\max}$ = 4%.

Postprocessing with a Vector of Two Intensity Measures

Similarly to the case of a single IM, changing to a vector of two IMs, one for each component, does not necessitate rerunning the dynamic analyses; only some sophisticated post-processing is required. Actually the definitions set forth in Vamvatsikos and Cornell (2002) do provide for a vector IM, while an appropriate framework has been developed on how to post-process and summarize such data by Vamvatsikos and Cornell (2005). To facilitate understanding we will take the reader through a detailed walkthrough of all the necessary steps.

There is a very important issue when selecting a secondary IM to form a vector by complementing our primary choice: Since the scaling is represented by the primary IM, say $S_{ax}(T_{1x},5\%)$, it would be redundant and often confusing if the secondary IM were also scalable rather than scaling-independent. That is not to say that one may not use another spectral value, but rather that it would be better if we normalized it by the primary IM to remove any redundant information. So we let our second IM be $S_{ay}(T_{1y},5\%)/S_{ax}(T_{1x},5\%)$ where the subscripts "*x*" and "*y*" refer to the *x* and *y* axis (and the corresponding ground motion components). Thus, we convey only the additional information that the new element brings in the vector with respect to our primary scalable IM.

Following a procedure similar to processing a single scalable IM, we use splines to interpolate the discrete IDA runs for each record versus the scalable IM of the vector (Vamvatsikos and Cornell 2002). We can then visualize the IDA curves versus the vector IM by plotting the EDP and the two single IMs in a 3D plot. In this case we will put the IMs on the *x*-*y* axes (representing the input) and place the EDP on the z-axis (it being the response). The results for $S_{ay}(T_{1y},5\%)/S_{ax}(T_{1x},5\%)$ as the secondary IM appear in Fig. 4a. The flatlines now extend upwards, parallel to the *z*-axis, rather than being the customary horizontal lines (Fig. 3a).

Summarizing the IDA curves cannot be performed with the usual cross-sectional fractiles at given levels of the vector, as we did for single IMs. That would require several values of EDP at each level of the non-scalable IM, practically impossible with a limited number of records. We use instead the symmetric-neighborhood running fractiles (Hastie and Tibshirani 1990) with a given window length to achieve the same purpose. The window length can be chosen by adopting a reasonable fraction of the sample size. In our case, we selected 33% of the sample size, i.e., we used the $0.33\times 26\approx 9$ symmetrically closest records to approximate the fractile value for each level of the non-scalable IM. The results are fractile IDA *surfaces*, rather than *lines*. For example, Fig. 4b shows the median surface corresponding to the IDA curves of Fig. 4a.

Now is the time to define limit-state capacities. It can be easily done using the same method as in 2D IDA curves. For example, for a limit-state at a specific $\theta_{s\max}$ value (an EDP-based rule) we only need to find the vector IM values for the given value of $\theta_{s\max}$. Imagine a horizontal plane (perpendicular to the *z*-axis) in Fig. 4a at the given $\theta_{s\max}$-value, cutting the IDA curves to produce 26 distinct capacity points, one for each record. These can be summarized in the same way as the demands, using running fractiles to compute fractile capacity *lines*. Taking

advantage of the established property that the *a*% fractile of IM|EDP is equal to the (100-*a*)% fractile of EDP|IM (Vamvatsikos and Cornell, 2004) we can also perform the same operation in an indirect way by taking advantage of the fractile IDA surfaces. Picture horizontal planes, each for a given $\theta_{s\max}$-value, cutting the IDA surface of Fig. 4b. The results can be visualized as contours of the fractile IDA surface, seen in Fig. 5a for the median IDA capacities given $\theta_{s\max}$. It is obvious that a high spectral ratio, i.e., a relatively high spectral acceleration at T_{1x} for the *y*-component of the earthquake has a severely negative effect for our structure. When the spectral ratio reduces from 2.5 to about 1.0 we see an instantaneous improvement in $S_{ax}(T_{1x},5\%)$ capacity at almost any limit-state (or EDP-level), which then again disappears for lower values of the spectral ratio. Apparently, when the two components have relatively similar spectral acceleration values at the corresponding fundamental periods T_{1x} and T_{2x} the frame gets a capacity boost, and it is allowed to reach the flatline at much higher intensities.

To further explain the meaning of these results, we have plotted in Fig. 5b the 16%, 50% and 84% capacity lines for the $\theta_{s\max}=4\%$ limit-state. These correspond to our best estimate of the 16%, 50% and 84% vector IM-value of the limit-state capacity. For example, if several records had a spectral ratio $S_{ay}(T_{1y},5\%)/S_{ax}(T_{1x},5\%)=2$, in order to reach $\theta_{s\max}=4\%$ for 16% of these records, we would need to equally scale both components so that $S_{ax}(T_{1x},5\%)=0.03$ g. If we scale to 0.05g instead, then 50% of the records will cause collapse while it takes a scaling to 0.08g to reach collapse for 84% of them. On the other hand, if the spectral ratio is only 1.0, then these scaling levels become quite higher, reaching 0.04g, 0.12g and 0.32g respectively. There is a consistent trend for higher capacities with decreasing spectral ratio, which peaks at a ratio of 1.0 and slightly decays for lower values. Clearly, the relative intensity of the, previously neglected, y-axis component is a very important parameter.

It is important to note that this additional information has come at a cost: We were forced to introduce summarization over windows rather than stripes. By introducing a secondary IM, we may have explained some of the variability in the capacities but we have also increased the dimensionality of the sample space, thus the data is sparser. Where we used to have 26 points for each level (stripe) of the scalable IM, we now have only a few points for whole regions of the unscalable IM.

Conclusions

The seismic performance of a 20-story space steel frame has been evaluated using Incremental Dynamic Analysis in three dimensions with biaxial seismic loading. It has proven to be a straightforward extension of the standard 2D IDA procedure that becomes highly interesting when a vector of two IMs, one for each component of the ground motion, is used instead of a single scalar. Forming a vector IM with the spectral accelerations of the two component of ground motion at the fundamental period in each direction helps explain much of the dispersion observed in the IDA results. Still, for the results to be uncovered, careful post-processing is needed that results in novel IDA fractile *surfaces* and capacity *lines* vis-à-vis the usual IDA fractile *lines* and capacity *points* expected from a 2D analysis. All in all, this is a promising methodology that can accurately quantify the seismic behavior of complex spatial structures

while accounting for biaxial seismic loading, thus decisively adding to current engineering intuition.

Acknowledgments

The author wishes to acknowledge the support of Professor C. A. Cornell towards visiting Stanford University during July 2005, where part of this research took place.

References

Foutch, D. A., and S.-Y. Yun, 2002. Modeling of steel moment frames for seismic loads, *Journal of Constructional Steel Research*, 58, 529–564.

Gupta, A., and H. Krawinkler, 1999. Seismic demands for performance evaluation of Steel moment resisting frame structures, *Report No. 132,* The John A. Blume Earthquake Engineering Research Center, Stanford University, Stanford, CA.

Hastie, T. J., and R. J. Tibshirani, 1990. *Generalized Additive Models*, Chapman & Hall, New York.

Vamvatsikos, D., and C. A. Cornell, 2002. Incremental dynamic analysis, *Earthquake Engineering and Structural Dynamics* 31(3), 491–514.

Vamvatsikos, D., and C. A. Cornell, 2004. Applied Incremental Dynamic Analysis, *Earthquake Spectra* 20 (2), 523–553.

Vamvatsikos, D., and C. A. Cornell, 2005. Developing efficient scalar and vector intensity measures for IDA capacity estimation by incorporating elastic spectral shape information, *Earthquake Engineering and Structural Dynamics* 34 (13), 1573–1600.

Vamvatsikos, D., and I. Sigalas, 2005. Seismic performance evaluation of a horizontally curved highway bridge using incremental dynamic analysis in 3D, *Proceedings of the 4th European Workshop on the Seismic Behavior of Irregular and Complex Structures,* Thessaloniki, Paper No. 33.

Wen, Y. K, and S.-H. Song, 2002. Structural reliability/redundancy under earthquakes. *ASCE Journal of Structural Engineering* 129 (1), 56–67.